

Effects of phase-gradient on the nonadiabatic dynamics and photon-phonon conversion in one-dimensional array of optomechanical cavities

Divya Mishra and Parvendra Kumar

Optics and Photonics Centre, Indian Institute of Technology Delhi, Hauz Khas, New Delhi, 110016
parvendra@opc.iitd.ac.in

Abstract: Manipulation of photonic and phononic coupling in the coupled resonators plays a crucial role in nonreciprocal devices and quantum transduction. In this work, we theoretically investigated how the phase of a driving laser introduces the phase-dependent coupling between photonic and phononic modes and affects the nonadiabatic dynamics of the eigenmodes and photon-phonon conversion in an array of coupled optomechanical cavities. We analyze the band structure of eigenmodes and show that the quick transfer of population between the eigenmodes takes place at the minimum energy gap, which can also be controlled via phase of the driving laser. We further show that the eigenmodes constitute the superposition of photonic and phononic modes, resulting from the optomechanical coupling between these modes. Moreover, the phase also enables the switching of the relative weights of photons and phonons in the eigenmodes. Finally, we investigate the effects of phase on the coherent conversion of photon-phonon in a finite-size array.

1. Introduction

The coupled optomechanical resonators constitute the key platforms for various applications in quantum computation and quantum information processing [1-8]. Generally, the optomechanical coupling between optical and vibrational modes arises due to the radiation pressure force [1]. This type of coupling has been realized in various systems including microwave-optomechanical circuits, microdisk resonators, and photonic crystal cavities [9-11]. The controllable degrees of freedom, such as coupling between optical and vibrational modes, resonator geometry, and external control via amplitude or phase modulation of the driving laser facilitate the observation and realization of many-body phenomena and practical applications [12-14]. Theoretical proposals and experimental demonstrations encompass the ground state cooling of mechanical modes, entanglement between mechanical and photonic modes [15-17], generation of squeezed states [18-20], single-phonon states [21], nonreciprocal quantum transport, quantum transduction and optomechanical quantum teleportation [22-24]. Particularly, one-dimensional array of optomechanical resonators provide a flexible platform to investigate the fundamental phenomena and many of these practical applications. Specifically, non-reciprocal photon transport, exceptional point based sensing, and topological photonics have been demonstrated with gauge fields generated by the modulated laser fields [25-29]. Furthermore, acoustic isolator, Su-Schrieffer-Heeger model, and coherent photon-phonon conversion have been realized with one-dimensional optomechanical arrays [30-32]. The control of nonadiabatic dynamics, photon-phonon conversion, and band structure is desirable for the realization of nonreciprocal transport and quantum transduction in quantum communications networks and distributed quantum computation [32-35].

In this work, we present a detailed investigation on the phase-induced modulation of nonadiabatic dynamics, band structure, and coherent conversion of photon-phonon. First, we compute the linearized Hamiltonian of the optomechanical array (OMA) and then calculated the eigenmodes and eigenvalues in the Fourier basis. We demonstrate that the coupling between optical and mechanical modes hybridizes the eigenmodes, resulting in a superposition of photonic and phononic modes. To investigate the nonadiabatic dynamics of eigenmodes, we employ the quantum Langevin equation and Magnus expansion methods. We show the phase-dependent nonadiabatic dynamics, particularly the quick transfer of population between the two eigenmodes at minimum energy gap position. We demonstrate that phase-tuning allows us to control the relative weights of photons and phonons in hybrid eigenmodes. Moreover, coherent photon-phonon conversion is also shown to be phase-dependent. It is worthwhile to mention that we model and simulate a similar system as used in Refs. [30, 31], however in contrast the present work focuses on the effects of phase modulation on the nonadiabatic dynamics, coherent photon-phonon conversion, and interpretation of nonadiabatic dynamics with the aid of band structure of eigenmodes.

2. Theoretical Model

The model of one-dimensional array of optomechanical resonators is shown in Fig. 1. Here, each site represents a single optomechanical resonator which supports a localized optical (blue circle) and mechanical (red circle) modes. The optomechanical coupling i.e. coupling between optical and mechanical modes is depicted by G . The hopping strengths between the two nearest optical and mechanical modes are represented by J and K , respectively. Additionally, optical mode at each site is driven by a phase modulated laser with site dependent phase, $e^{in\theta}$.

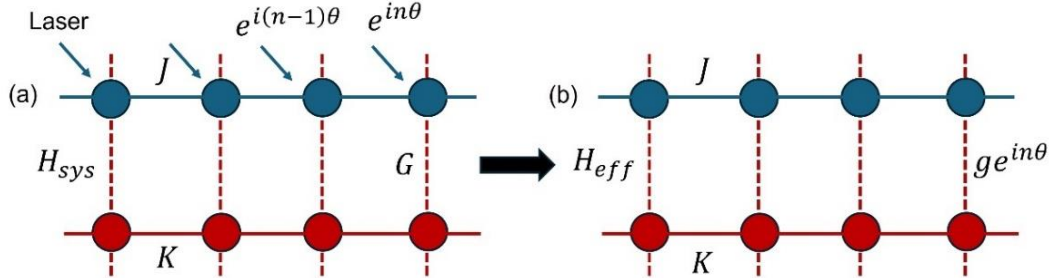


Fig. 1 (color online) Schematic of the optomechanical array. (a) Each site consists of a coupled optical mode (blue circle) and a phonon mode (red circle) with coupling strength G . The hopping strengths between nearest neighbour optical and phonon modes are represented by J and K , respectively. The laser driving of optical modes with site dependent phase $e^{in\theta}$ transforms the bare Hamiltonian H_{sys} into an effective Hamiltonian H_{eff} with an enhanced and position dependent optomechanical coupling $ge^{in\theta}$ as shown in (b).

This position dependent phase breaks time-reversal symmetry [30] and introduces a position dependent effective coupling between optical and mechanical modes as shown in Fig. 1(b). The Hamiltonian of OMA shown in Fig. 1(a) reads as [1, 30]:

$$H_{sys} = H_s + H_t, \quad (1)$$

$$H_s = \sum_n \omega_c a_n^\dagger a_n + \omega_m b_n^\dagger b_n - G a_n^\dagger a_n (b_n^\dagger + b_n) + \Omega_d \cos(\omega_d t + n\theta) (a_n^\dagger + a_n), \quad (2a)$$

$$H_t = -J \sum_n (a_n^\dagger a_{n+1} + a_{n+1}^\dagger a_n) - K \sum_n (b_n^\dagger b_{n+1} + b_{n+1}^\dagger b_n) \quad (2b)$$

Here, H_s and H_t represent the Hamiltonians of each sites and tunnelling between them, respectively, G represents a vacuum coupling rate. The bosonic operator a_n (b_n) destroy a photonic (phononic) excitation with energy ω_c (ω_m), Ω_d , ω_d , and θ represent the Rabi frequency, frequency, and phase of the driving laser, respectively. We transform H_{sys} in a frame rotating with angular frequency ω_d together with rotating wave approximation. The linearized effective Hamiltonian reads as [1]:

$$H_{eff} = -\frac{\Delta}{2} \sum_n a_n^\dagger a_n + \frac{\omega_m}{2} \sum_n b_n^\dagger b_n - J \sum_n a_n^\dagger a_{n+1} - K \sum_n b_n^\dagger b_{n+1} - g \sum_n e^{-in\theta} a_n^\dagger b_n + h.c., \quad (3)$$

where $g = G\alpha$ is the optomechanical coupling strength enhanced by a factor of $\alpha = \sqrt{n_o}$, where n_o is the average number of photons in the optical cavity mode. This reads as $\alpha = \Omega_d / \left[\left(\Delta + \frac{i\kappa}{2} \right) + 2J \cos\theta + G(\beta + \beta^*) \right]$, $\Delta = (\omega_d - \omega_c)$ and $|\beta|^2$ represents the average phonon number in the mechanical mode, where $\beta = G|\alpha|^2 / \left[\left(\omega_m - \frac{i\gamma_m}{2} \right) - 2K \right]$, κ and γ_m represent the decay rates of optical and mechanical modes, respectively.

3. Results and Discussions

For calculating the band structure of OMA, we transform the Hamiltonian H_{eff} in the Fourier basis by defining the corresponding creation and annihilation operators as $\begin{pmatrix} a_n \\ b_n \end{pmatrix} = \sum_k e^{-inkd} \begin{pmatrix} a_k e^{-in\theta} \\ b_k \end{pmatrix}$, k and d represent the wavenumber and lattice constant, respectively. The Fourier-transformed Hamiltonian H_k is given as:

$$H_k = \begin{pmatrix} -\Delta - 2J \cos(kd + \theta) & -g \\ -g & \omega_m - 2K \cos(kd) \end{pmatrix} \quad (4)$$

The Hamiltonian is an effective approximation for sufficiently large lattices and periodic boundary conditions [30]. The eigenvalues of H_k are $\omega_k(\pm) = (\Omega - \xi)/2 \pm \sqrt{g^2 + \delta^2}$, $\Omega = \omega_m - 2K \cos(kd)$, $\xi = \Delta + 2J \cos(kd + \theta)$, and $\delta = (\Omega + \xi)/2$. The eigenmodes corresponding to $\omega_k(+)$ and $\omega_k(-)$ are $A_k = \frac{-g}{\sqrt{g^2 + (\delta + \sqrt{g^2 + \delta^2})^2}} a_k + \frac{\delta + \sqrt{g^2 + \delta^2}}{\sqrt{g^2 + (\delta + \sqrt{g^2 + \delta^2})^2}} b_k$ and $B_k =$

$\frac{-g}{\sqrt{g^2 + (\delta - \sqrt{g^2 + \delta^2})^2}} a_k + \frac{\delta - \sqrt{g^2 + \delta^2}}{\sqrt{g^2 + (\delta - \sqrt{g^2 + \delta^2})^2}} b_k$, respectively. Clearly, both eigenmodes consist superposed optical and mechanical modes and therefore they are termed as hybrid modes. The relative weights of photons and phonons composing the eigenmode A_k are given as $\alpha_A = \frac{-g}{\sqrt{g^2 + (\delta + \sqrt{g^2 + \delta^2})^2}}$ and $\beta_A = \frac{\delta + \sqrt{g^2 + \delta^2}}{\sqrt{g^2 + (\delta + \sqrt{g^2 + \delta^2})^2}}$, respectively. Similarly for eigenmode B_k , these are

given as $\alpha_B = \frac{-g}{\sqrt{g^2 + (\delta - \sqrt{g^2 + \delta^2})^2}}$ and $\beta_B = \frac{\delta + \sqrt{g^2 + \delta^2}}{\sqrt{g^2 + (\delta + \sqrt{g^2 + \delta^2})^2}}$, respectively. Note that the eigenmodes can also be written in the compact form as $\begin{pmatrix} A_k \\ B_k \end{pmatrix} = R_k(g) \begin{pmatrix} a_k \\ b_k \end{pmatrix}$, where $R_k(g) = \begin{pmatrix} \alpha_A & \beta_A \\ \alpha_B & \beta_B \end{pmatrix}$.

A. Nonadiabatic dynamics of eigenmodes

For investigating the eigenmodes dynamics following a sudden change in the optomechanical coupling from g to $-g$ over a period of time t_q , $g(t) = g \left(1 - \frac{2t}{t_q}\right)$, here t_q specifies how quickly the coupling is changed from g to $-g$. First, we compute time propagator $S_k(g(t))$ by solving the equations of motion for $a_k(g(t))$ and $b_k(g(t))$ with first order Magnus expansion method [36] as given in the appendix A, which reads as:

$$S_k(g(t)) = \begin{pmatrix} \cos\eta(t) - i \frac{\phi(t)}{\eta(t)} \sin\eta(t) & i \frac{\theta(t)}{\eta(t)} \sin\eta(t) \\ i \frac{\theta^*(t)}{\eta(t)} \sin\eta(t) & \cos\eta(t) - i \frac{\phi(t)}{\eta(t)} \sin\eta(t) \end{pmatrix}, \quad (5)$$

$$\begin{pmatrix} a_k(g(t)) \\ b_k(g(t)) \end{pmatrix} = S_k(g(t)) \begin{pmatrix} a_k \\ b_k \end{pmatrix} \quad (6)$$

where, $\eta(t) = \sqrt{|\theta(t)|^2 + \phi^2(t)}$, $\theta(t) = \frac{g}{2\delta} \left[i(e^{2i\delta t} - 1) - \frac{2ite^{2i\delta t}}{t_q} + \frac{1}{\delta t_q} (e^{2i\delta t} - 1) \right]$, and $\phi(t) = \frac{g^2}{4t_q\delta^3} \xi + \frac{g^2}{t_q\delta} \zeta + \frac{g^2}{2\delta} \chi$. Here, $\xi = \left[1 - \cos(2\delta t) + \frac{2t}{t_q} \cos(2\delta t) - \frac{1}{t_q\delta} \sin(2\delta t) \right]$, $\zeta = \left[\frac{t^2}{2} - \frac{2t^3}{3t_q} \right]$, and $\chi = \left[t - \frac{t^2}{t_q} - \frac{\sin(2\delta t)}{2\delta} + \frac{1}{t_q\delta} t \sin(2\delta t) + \frac{1}{2t_q\delta^2} \{ \cos(2\delta t) - 1 \} \right]$. We use $S_k(g(t))$, a_k and b_k for calculating the temporal dynamics of eigenmodes as follows:

$$\begin{pmatrix} A_k(g(t), t) \\ B_k(g(t), t) \end{pmatrix} = R_k(g(t)) S_k(g(t)) \begin{pmatrix} a_k \\ b_k \end{pmatrix} \quad (7)$$

$$\begin{pmatrix} A_k(g(t), t) \\ B_k(g(t), t) \end{pmatrix} = R_k(g(t)) S_k(g(t)) R_k^{-1}(g(0)) \begin{pmatrix} A_k \\ B_k \end{pmatrix}, \quad (8)$$

Furthermore, we compute the steady state population of eigenmodes, which are given as $N_{th}(A_k) = \frac{(1-p_A)\Gamma n_{th}}{p_A\kappa + (1-p_A)\Gamma}$ and $N_{th}(B_k) = \frac{p_A\Gamma n_{th}}{(1-p_A)\kappa + p_A\Gamma}$. The detailed calculation is given in the appendix B, here, $p_A = \alpha_A^2$, $\kappa(\Gamma)$ represent the decay of optical (mechanical) mode and n_{th} is the average number of thermal phonons in heat bath.

Finally, we calculate the eigenmode population $\langle A_k^\dagger A_k(g(t)) \rangle$ and $\langle B_k^\dagger B_k(g(t)) \rangle$ using Eq. 8 together with Eq. 5 and show their dynamics in Figs. 6 and 7. It is worthwhile to mention that the nature of evolution depends on the value of t_q , for $t_q \gg \frac{1}{\Delta\omega_k}$ the evolution would be adiabatic, while for $t_q \ll \frac{1}{\Delta\omega_k}$ it would be nonadiabatic, $\Delta\omega_k$ is the energy gap between two the bands.

We compute the eigenmode population $N(A_k) = \langle A_k^\dagger A_k(g(t)) \rangle / n_{th}$ and $N(B_k) = \langle B_k^\dagger B_k(g(t)) \rangle / n_{th}$ from Eq. 6 together with Eq. 7. The net excitation of eigenmodes is defined as $N_q(A_k) = (\langle A_k^\dagger A_k(g(t)) \rangle - N_{th}(A_k)) / n_{th}$ and $N_q(B_k) = (\langle B_k^\dagger B_k(g(t)) \rangle - N_{th}(B_k)) / n_{th}$. We show the nonadiabatic dynamics of eigenmodes in Figs. 2 and 3. It can be observed from Fig. 2(a) that in contrast to the adiabatic dynamics, the transfer of population occurs between the two eigenmodes. There is an excitation of mode B_k for $\theta = 0$, while it reverses to the excitation of mode A_k for $\theta = \pi$, as shown in Fig. 2(b).

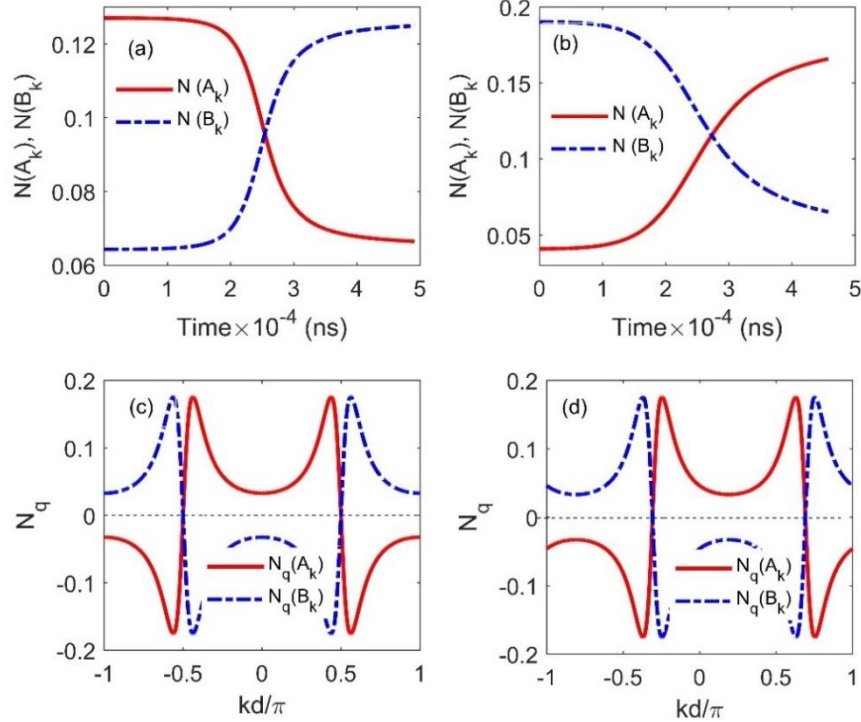


Fig. 2 (color online) Dynamics of eigenmodes due to the sudden change of optomechanical coupling from positive to negative: g to $-g$ over a time $t_q = \frac{10^{-4}}{\Delta\omega_k}$. (a) $kd = 0.48\pi$ and $\theta = 0$, (b) $kd = 0.48\pi$ and $\theta = \pi$. Net excitation in eigenmodes: (c) $\theta = \pi$, and (d) $\theta = 0.8\pi$. The value of other simulation parameters is $\omega_m = 4.3$ GHz, $J = 0.5$ GHz, $g = 0.1$ GHz, and $K = 0.2$ GHz.

Next in Fig. 2(c), the net excitation of eigenmodes is shown for $\theta = \pi$. Nonadiabatic dynamics manifests itself through the exchange of population between the eigen modes. The transfer of population is very fast around $kd = \pm 0.5\pi$ due to the lowest energy gap as can be observed in Fig. 4(b). The similar trend of excitations can be observed in Fig 2(d) for $\theta = 0.8\pi$; however, the dominant excitations are now shifted to $kd = -0.4\pi$ and 0.6π . This happens due to the shifting of minimum energy gap as shown in Fig. 4(d).

Next, we show the net excitations in the eigenmodes for $J, K > g$. It is clear from Figs. 3(a) and 3(d) that for $\theta = 0$ and π , the transfer of net excitations occurs at $kd = \pm \pi/2$ due to the lowest energy gap thereat. However, for $\theta = \pi$, the transfer of population takes place from eigen mode A_k to eigen mode B_k and vice versa at $kd = -\pi/2$ and $kd = \pi/2$, respectively.

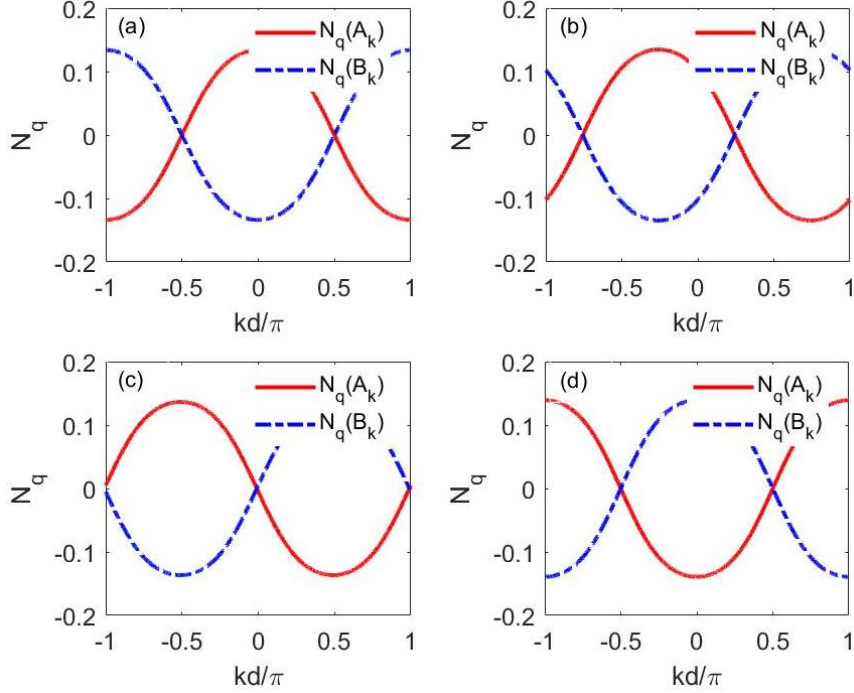


Fig. 3 (color online) Net excitation in the eigen modes for $t_q = \frac{10^{-4}}{\Delta\omega_k}$ (a) $\theta = 0$, (b) $\theta = \pi/4$, (c) $\theta = \pi/2$, and (d) $\theta = \pi$. The value of other simulation parameters is $g = 0.086 \text{ GHz}$, $\omega_m = 4.3 \text{ GHz}$, $J = 0.043 \text{ GHz}$, and $K = 0.0013 \text{ GHz}$.

For $\theta = \pi/4$, the fast transfer of net excitation is now shifted to the lowest energy gap at $kd = -0.87\pi$ and 0.13π (see Fig. 7(a)). Similarly, Fig. 3(c) shows the phase-induced shifting of fast transfer of net excitations to $kd = 0, \pm\pi$. We found that the phase-dependent energy gap plays an important role in the nonadiabatic dynamics of eigen modes, therefore for clarity, next we show the phase dependence of band structure.

B. Control of band structure and eigenmodes

Here, we show the effects of the phase-induced modulation of band structure of eigenmodes. Fig. 4 shows that how the energy gap between the hybrid eigenmodes depend on the normalized wavenumber at different values of g and θ . It is clear from Fig. 4 (a) that the energy gap between the two modes is maximum at $kd = 0$, while it vanishes at the two crossings $kd = \pm\pi/2$. However, for $g = 0.1 \text{ GHz}$ in Fig. 4(b), the energy gap opens up with avoided crossings at $kd = \pm\pi/2$. The band structure changes significantly for $\theta \neq 0$ with a few minima and maxima as shown in Figs. 4(c) and 4 (d). Moreover, for $\theta = 0.8\pi$, minimum energy gap becomes asymmetric and shifts toward the higher value of ω_k at $kd = 0.6\pi$, while it shifts toward the lower value of ω_k at $kd = -0.4\pi$. Such a shifting of minimum energy gap is the underlying reason of fast transfer of population between eigenmodes shown in Fig. 2(d).

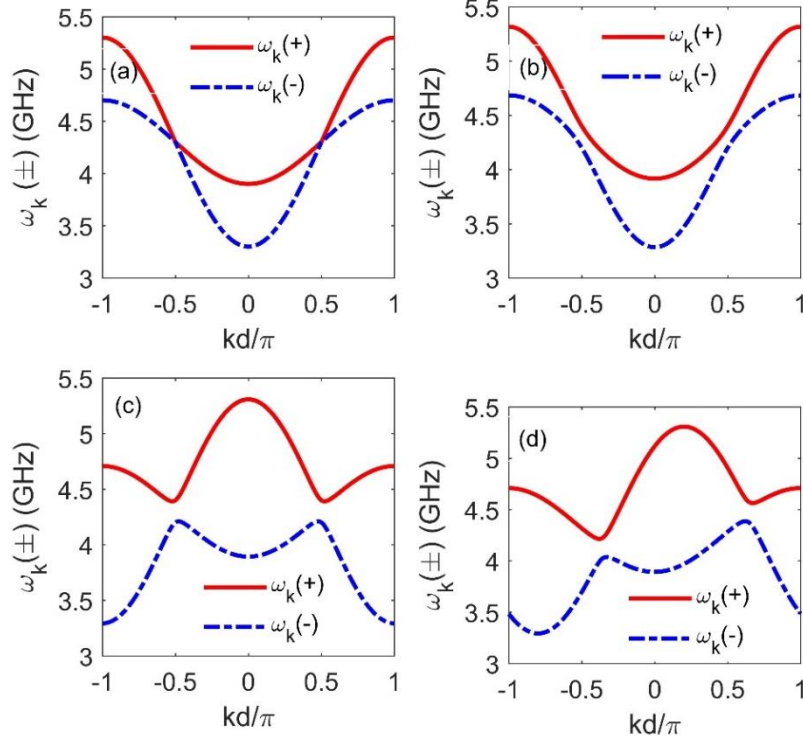


Fig. 4 (color online) Energy of the hybrid eigenmodes as a function of normalized wavenumber for detuning $\Delta = -\omega_m$. (a) $g = 0$ and $\theta = 0$, (b) $g = 0.1 \text{ GHz}$ and $\theta = 0$, (c) $g = 0.1 \text{ GHz}$ and $\theta = \pi$, and (d) $g = 0.1 \text{ GHz}$ and $\theta = 0.8\pi$. The value of other simulation parameters is $\omega_m = 4.3 \text{ GHz}$, $J = 0.5 \text{ GHz}$, and $K = 0.2 \text{ GHz}$.

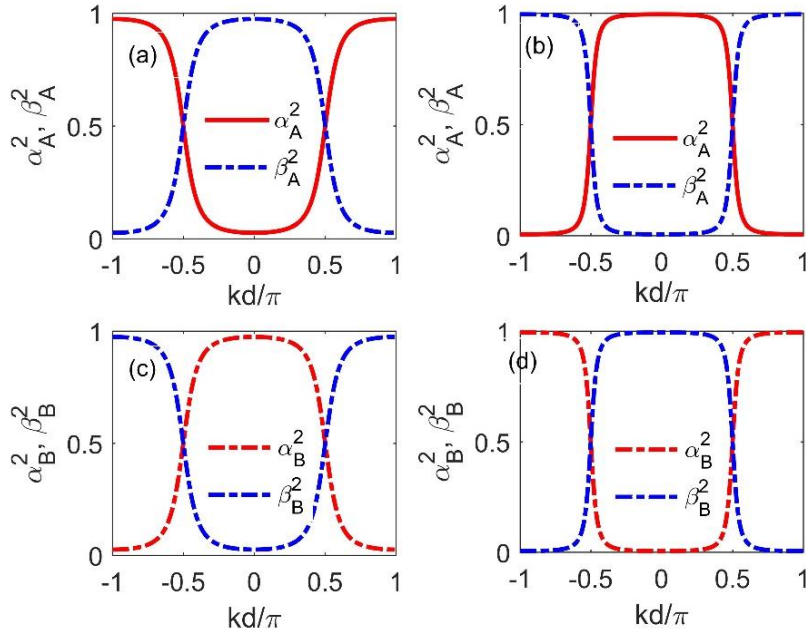


Fig. 5 (color online) The relative weights of photons and phonons composing the hybrid eigenmodes. (a) α_A^2 and β_A^2 for $g = 0.1 \text{ GHz}$ and $\theta = 0$, (b) α_A^2 and β_A^2 for $g = 0.1 \text{ GHz}$ and $\theta = \pi$, (c) α_B^2 and β_B^2 for $g = 0.1 \text{ GHz}$ and $\theta = 0$, and (d) α_B^2 and β_B^2 for $g = 0.1 \text{ GHz}$ and $\theta = \pi$. The value of other simulation parameters is same as employed in Fig. 2.

In Fig. 5, we show the relative weight of photons and phonons composing the hybrid eigenmodes, A_k and B_k as a function of normalized wavenumber at two distinct phases, $\theta = 0$ and π . The eigen mode A_k is mostly phononic in the middle, $-\pi/2 < kd < \pi/2$, and outside it is mostly photonic as can be observed in Fig. 5(a). However, the swapping of relative weights of photons and phonons do occur for $\theta = \pi$, specifically, A_k becomes mostly photonic in the middle, $-\pi/2 < kd < \pi/2$, and outside it is mostly phononic. Similarly, the swapping of relative weights happens in eigenmode B_k for $\theta = \pi$ as shown in Fig. 5(c) and 5(d).

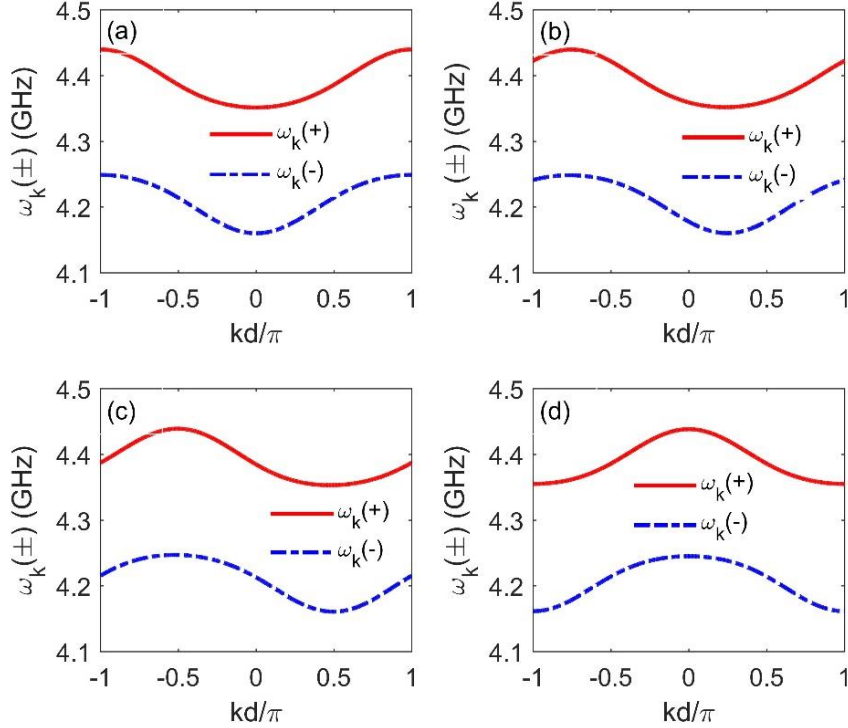


Fig. 6 (color online) Energy of the hybrid eigenmodes as a function of normalized wavenumber for detuning $\Delta = -\omega_m$. (a) $\theta = 0$, (b) $\theta = \pi/4$, (c) $\theta = \pi/2$, and (d) $\theta = \pi$. The value of other simulation parameters is $g = 0.086 \text{ GHz}$, $\omega_m = 4.3 \text{ GHz}$, $J = 0.043 \text{ GHz}$, and $K = 0.0013 \text{ GHz}$.

In Fig. 4, we show the phase dependent band structure for $J, K > g$. However, for generality and comparative analysis, we investigate the band structure in the opposite regime, $J, K < g$. It can be observed from Fig. 6 that the energy gap changes as a function of wavenumber and the location of the gap minima also depends on the value of θ . Specifically, the gap minima appear at $kd = \pm\pi/2$ for $\theta = 0$ and π , while it shifts toward $kd = -0.75\pi$ and 0.25π for $\theta = \pi/4$ and toward $kd = 0$ and $\pm\pi$ for $\theta = \pi/2$. The phase-induced shifting of lowest energy gap enables the shifting of fast transfer of population, which is shown in Fig. 3. For clarity, the variation of energy gap in both cases, $J, K < g$ and $J, K > g$ is shown in Figs. 7(a) and 7(b), respectively. The energy gap minima and maxima are obtained at 0.172 GHz and 0.194 GHz for $\theta = \pi$, as shown in Fig 7(a). Also, it is clear that energy gap maxima values are slightly different for $\theta = 0, \pi/4$, and $\pi/2$. For $J, K > g$, the minimum of the gap also appears at $kd = \pm\pi/2$ for $\theta = 0$ and

π . However, it shifts to $kd = -0.87\pi$ and 0.13π for $\theta = \pi/4$, and $kd = -0.13\pi$ and 0.87π for $\theta = \pi/2$. The peak value of energy gap for each chosen θ is substantially different and greater than those are shown in Fig. 7(a). The phase dependent controllability of the minimum energy gap position and peak value of the energy gap manifest themselves in the nonadiabatic dynamics of eigenmodes as shown in Figs. 2 and 3.

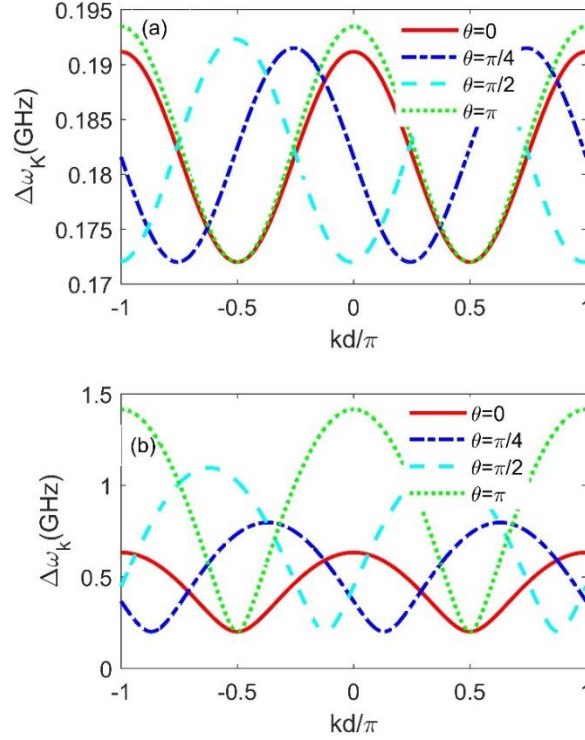


Fig. 7 (color online) Energy gap as a function of normalized wavenumber for $\theta = 0$ (solid red line), $\pi/4$ (dashed-dotted blue line), $\pi/2$ (dashed cyan line), and π (dotted green line). (a) $g = 0.086$ GHz, $\omega_m = 4.3$ GHz, $J = 0.043$ GHz, and $K = 0.0013$ GHz, (b) $g = 0.1$ GHz, $\omega_m = 4.3$ GHz, $J = 0.5$ GHz, and $K = 0.2$ GHz.

C. Coherent photon-phonon conversion

Next, we investigate the phase-dependent photon-phonon conversion in a four- and five-site arrays of coupled optomechanical cavities by numerically solving the quantum master equation, given in appendix B. We termed the first and fourth (fifth in Fig. 10) sites as input and output sites. We can see in Fig. 8(a) and (b) how phonons change into photons at the input $\langle a_1^\dagger a_1 \rangle$ and output $\langle a_4^\dagger a_4 \rangle$ sites for initially populated, output $\langle b_4^\dagger b_4 \rangle = 1$ and input $\langle b_1^\dagger b_1 \rangle = 1$, phononic modes. Similarly, Figs. 8(c) and (d) illustrate the conversion of photons into phonons at the input $\langle b_1^\dagger b_1 \rangle$ and output $\langle b_4^\dagger b_4 \rangle$ sites if initially photonic modes are occupied. It is clear from Fig. 8 that for phase $\theta = 0$, the dynamics of average photon and phonon number are identical irrespective of the launching sites of photons and phonons.

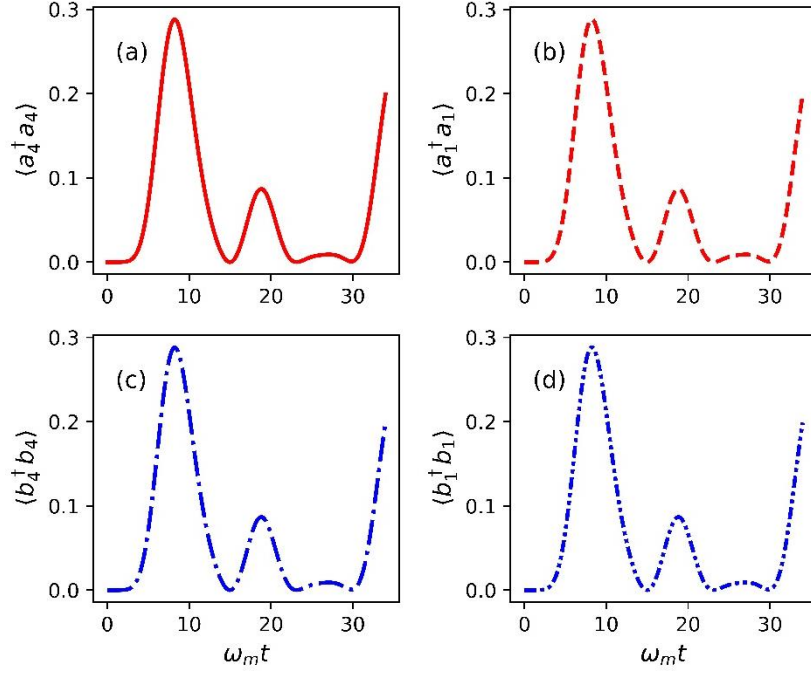


Fig. 8 (color online) Coherent photon-phonon conversion in a four sites optomechanical array for $\kappa = 0.01\omega_m$, $\Gamma = 0.001\omega_m$, and $\theta = 0$ (a) $\langle b_1^\dagger b_1 \rangle = 1$, (b) $\langle b_4^\dagger b_4 \rangle = 1$, (c) $\langle a_1^\dagger a_1 \rangle = 1$, and (d) $\langle a_4^\dagger a_4 \rangle = 1$. The other parameters are same as used in Fig. 2.

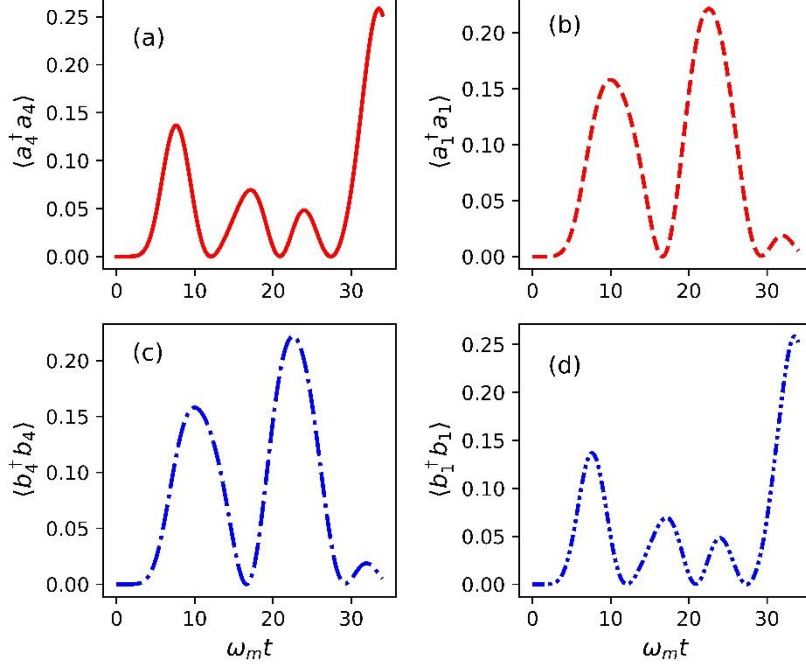


Fig. 9 (color online) Coherent photon-phonon conversion in a four sites optomechanical array for $\kappa = 0.01\omega_m$, $\Gamma = 0.001\omega_m$, and $\theta = \pi$ (a) $\langle b_1^\dagger b_1 \rangle = 1$, (b) $\langle b_4^\dagger b_4 \rangle = 1$, (c) $\langle a_1^\dagger a_1 \rangle = 1$, and (d) $\langle a_4^\dagger a_4 \rangle = 1$. The other parameters are same as used in Fig. 2.

However, it is evident from Fig. 9 that for phase $\theta = \pi$, the dynamics of average photon and phonon number are no longer identical. Specifically, for an initially populated first phononic site, i.e. $\langle b_1^\dagger b_1 \rangle = 1$, the average photon number at fourth site is maximum (0.26) at $\omega_m t = 33$, while minimum (0.01) at first site for $\langle b_4^\dagger b_4 \rangle = 1$. Fig. 9 (c) and (d) show similar trends of phase-dependent conversion of photons into phonons. Therefore, the conversion and propagation of photons (phonons) between the first and fourth site shows a strong phase dependence. For the chosen parameters, the maximum efficiency of photon-phonon conversion is found to be 26% as shown in Fig. 9(a) and 9(d).

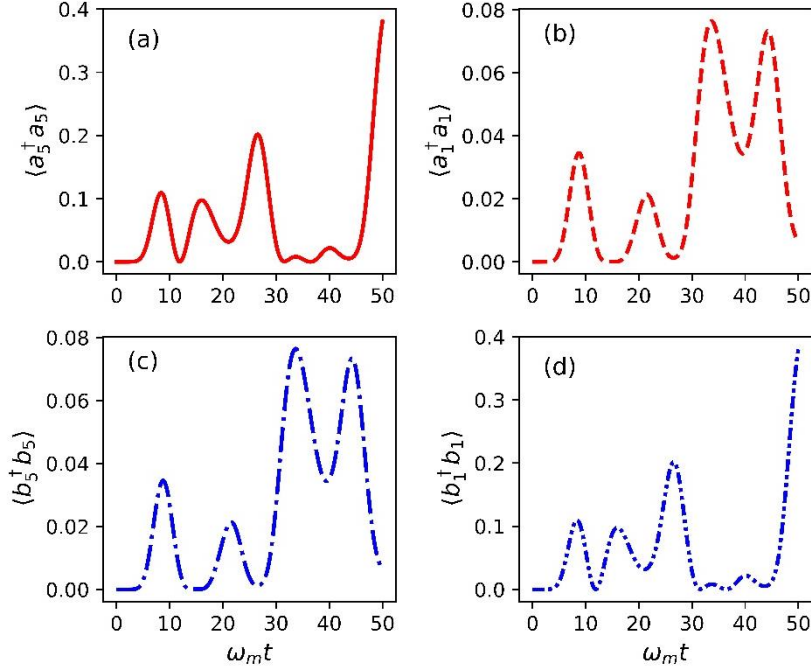


Fig. 10 (color online) Coherent photon-phonon conversion in a five sites optomechanical array for $\kappa = 0.01\omega_m$, $\Gamma = 0.001\omega_m$, and $\theta = \pi$ (a) $\langle b_1^\dagger b_1 \rangle = 1$, (b) $\langle b_4^\dagger b_4 \rangle = 1$, (c) $\langle a_1^\dagger a_1 \rangle = 1$, and (d) $\langle a_4^\dagger a_4 \rangle = 1$. The other parameters are same as used in Fig. 2.

Finally, we investigate the photon-phonon conversion in a five-site array for $\theta = \pi$. Like Fig. 9, the conversion and propagation of photons (phonons) between the first and fifth sites shows a strong dependence on the phase of the driving laser. For an initially populated first phononic site, $\langle b_1^\dagger b_1 \rangle = 1$, the average photon number at fifth site is maximum (0.38) at $\omega_m t = 50$, while it is minimum (0.01) at first site for $\langle b_4^\dagger b_4 \rangle = 1$. The conversion of photons into phonons follows a similar trend as shown in Figs. 10 (c) and (d). However, with the same parameters as used in Fig. 9, the maximum efficiency of photon-phonon conversion in a five-site array gets enhanced and found to be greater than 38% as shown in Fig. 10(a) and 10(d). We anticipate that the phase dependence of photon-phonon conversion arises due to the interference between the different paths that a converted photon (phonon) can traverse to reach the first or fifth site [37]. However, to substantiate this, further analytical and simulation studies are required.

4. Conclusion

In conclusion, we have investigated the effects of phase-induced modulation of nonadiabatic dynamics of eigenmode population and coherent conversion of photon-phonons in an array of optomechanical resonators. We demonstrated that by manipulating the phase of the driving laser, we can control the transfer of net excitations generated by the nonadiabatic evolution of eigenmodes. It is shown that the eigenmodes constitute the superposition of photonic and phononic modes, and their relative weights can be switched by appropriately controlling the phase. Furthermore, we have demonstrated the phase dependence of photon-phonon conversion at both the input and output sites in a four- and five-site array, the later demonstrates the greater conversion efficiency. This work may be useful for applications involving the quantum transduction and transport of photons and phonons in coupled resonators.

Acknowledgements

P. K. gratefully acknowledge the new faculty seed grant from Indian Institute of Technology Delhi.

APPENDIX A: EQUATION OF MOTIONS FOR PHOTONIC AND PHONONIC MODES

The time dependent Hamiltonian in Fourier basis is given as:

$$H_k(t) = \begin{pmatrix} -\Delta(k) & -g(t) \\ -g(t) & \Omega(k) \end{pmatrix} \quad (\text{A1})$$

We consider the following ansatz wave function:

$$\psi_k(t) = a_k(g(t))e^{i\Delta(k)t}\psi_a + b_k(g(t))e^{-i\Omega(k)t}\psi_b, \quad (\text{A2})$$

here, $\Delta(k) = \Delta + 2J \cos(kd + \theta)$, $\Omega(k) = \omega_m - 2K \cos(kd)$, $a_k(t)$, and $b_k(t)$ are the probability amplitudes of the photonic and phononic modes. To derive the equation of motion we use the time dependent Schrödinger equation.

$$i\hbar \frac{d\psi_k(t)}{dt} = H_k(t)\psi_k(t) \quad (\text{A3})$$

From Eqs. A1, A2, and A3, we get the following equations of motion:

$$\dot{a}_k(g(t)) = ig(t)b_k(g(t))e^{-i\Delta'(k)t} \quad (\text{A4})$$

$$\dot{b}_k(g(t)) = ig(t)a_k(g(t))e^{i\Delta'(k)t}, \quad (\text{A5})$$

where, $\Delta'(k) = \Delta(k) + \Omega(k)$.

APPENDIX B: STEADY STATE POPULATION OF EIGEN MODES

We follow the Ref. [31] for deriving the steady state population of eigenmodes. The equations of motion for $a_k(t)$ and $b_k(t)$ with constant optomechanical coupling strength is derived using Hamiltonian given by Eq. 4 and employing Heisenberg-Langevin equations, which reads as:

$$\frac{d}{dt} \begin{pmatrix} a_k \\ b_k \end{pmatrix} = \begin{pmatrix} i\Delta(k) - \frac{\kappa}{2} & ig \\ ig & -i\Omega(k) - \frac{\Gamma}{2} \end{pmatrix} \begin{pmatrix} a_k \\ b_k \end{pmatrix} + \begin{pmatrix} \sqrt{\kappa}a_{in} \\ \sqrt{\Gamma}b_{in} \end{pmatrix}, \quad (\text{A6})$$

here, κ and Γ are the decay rates of photonic and phononic modes, while a_{in} and b_{in} are the input noise operators of photonic and phononic modes. For $g = 0$, it is straightforward to find the solution of $b_k(t)$ from Eq. A6. It reads as

$$b_k(t) = e^{-(i\Omega(k) + \frac{\Gamma}{2})t} \left[b_k(0) + \sqrt{\Gamma} \int_0^t dt' e^{-(i\Omega(k) + \frac{\Gamma}{2})t'} b_{in}(t') \right] \quad (\text{A7})$$

The Heisenberg-Langevin equations of motion for eigen modes, A_k and B_k reads as follows:

$$\frac{d}{dt} \begin{pmatrix} A_k \\ B_k \end{pmatrix} = \begin{pmatrix} -i\omega_k(+) - \frac{\kappa_A}{2} & 0 \\ 0 & -i\omega_k(-) - \frac{\kappa_B}{2} \end{pmatrix} \begin{pmatrix} A_k \\ B_k \end{pmatrix} + \begin{pmatrix} A_{in} \\ B_{in} \end{pmatrix} \quad (\text{A8})$$

κ_A and κ_B represent the decay rates, while A_{in} and B_{in} are the linear superposition of a_{in} and b_{in} . We calculate the κ_A and κ_B as the first-order perturbation to matrix M , given below, without decay rates.

$$M = \begin{pmatrix} i\Delta(k) & ig \\ ig & -i\Omega(k) \end{pmatrix} + \begin{pmatrix} -\frac{\kappa}{2} & 0 \\ 0 & -\frac{\Gamma}{2} \end{pmatrix} \quad (\text{A9})$$

From Eq. A8, the population of eigen modes A_k and B_k can be calculated similar to the isolated mode b_k in Eq. A7. Following the calculations, we get

$$\langle A_k^\dagger A_k(t) \rangle = e^{-\kappa_A t} \left[\langle A_k^\dagger A_k(0) \rangle + \int_0^t \int_0^t dt' dt'' e^{\kappa_A(t'+t'')/2} e^{\omega_k(+)(t'-t'')} \langle A_{in}^\dagger(t') A_{in}(t'') \rangle \right] \quad (\text{A10})$$

$$\begin{pmatrix} A_{in}(t) \\ B_{in}(t) \end{pmatrix} = \begin{pmatrix} \alpha_A & \beta_A \\ \alpha_B & \beta_B \end{pmatrix} \begin{pmatrix} \sqrt{\kappa}a_{in}(t) \\ \sqrt{\Gamma}b_{in}(t) \end{pmatrix} \quad (\text{A11})$$

From Eq. A11, $\langle A_{in}^\dagger(t') A_{in}(t'') \rangle$ is calculated and reads as follows:

$$\langle A_{in}^\dagger(t') A_{in}(t'') \rangle = \alpha_A^2 \kappa \langle a_{in}^\dagger(t') a_{in}(t'') \rangle + \beta_A^2 \Gamma \langle b_{in}^\dagger(t') b_{in}(t'') \rangle, \quad (\text{A12})$$

here, $\alpha_A^2 + \beta_A^2 = 1$. Under Markov approximation with optical bath at zero temperature, we get

$$\langle a_{in}^\dagger(t') a_{in}(t'') \rangle = 0, \langle b_{in}^\dagger(t') b_{in}(t'') \rangle = n_{th} \delta(t' - t''), \quad (\text{A13})$$

here, n_{th} is the average number of thermal phonons.

From Eqs. A10, A12, and A13, we get,

$$\langle A_k^\dagger A_k(t) \rangle = e^{-\kappa_A t} \left[\langle A_k^\dagger A_k(0) \rangle + \int_0^t \int_0^t dt' dt'' e^{\kappa_A(t'+t'')/2} e^{\omega_k(+)(t'-t'')} \beta_A^2 \Gamma n_{th} \delta(t' - t'') \right] \quad (\text{A14})$$

$$\langle A_k^\dagger A_k(t) \rangle = e^{-\kappa_A t} \left[\langle A_k^\dagger A_k(0) \rangle + \int_0^t dt' e^{\kappa_A t'} \beta_A^2 \Gamma n_{th} \right] \quad (\text{A15})$$

$$\langle A_k^\dagger A_k(t) \rangle = e^{-\kappa_A t} \left[\langle A_k^\dagger A_k(0) \rangle + \beta_A^2 \Gamma n_{th} \left(\frac{e^{\kappa_A t} - 1}{\kappa_A} \right) \right] \quad (\text{A16})$$

$$\langle A_k^\dagger A_k(t) \rangle_{t \rightarrow \infty} = \frac{\beta_A^2 \Gamma n_{th}}{\kappa_A}, \text{ where } \kappa_A = \alpha_A^2 \kappa + \beta_A^2 \Gamma$$

$$\langle A_k^\dagger A_k(t) \rangle_{t \rightarrow \infty} = \frac{(1 - \alpha_A^2) \Gamma n_{th}}{\alpha_A^2 \kappa + (1 - \alpha_A^2) \Gamma} \quad (\text{A17})$$

After repeating the same procedure, we get the steady state population of eigen mode B_k as:

$$\langle B_k^\dagger B_k(t) \rangle_{t \rightarrow \infty} = \frac{\alpha_A^2 \Gamma n_{th}}{(1 - \alpha_A^2) \kappa + \alpha_A^2 \Gamma} \quad (\text{A18})$$

We use the following quantum master equation in Lindblad form for calculating the average population: $\langle a_n^\dagger a_n \rangle = \text{tr}(a_n^\dagger a_n \rho)$, $\langle b_n^\dagger b_n \rangle = \text{tr}(b_n^\dagger b_n \rho)$

$$\frac{d\rho}{dt} = -i[H_{eff}, \rho] + \frac{\kappa}{2} \sum_n (2a_n \rho a_n^\dagger - a_n^\dagger a_n \rho - \rho a_n^\dagger a_n) + \frac{\Gamma}{2} \sum_n (2b_n \rho b_n^\dagger - b_n^\dagger b_n \rho - \rho b_n^\dagger b_n) \quad (\text{A19})$$

References

- [1] M. Aspelmeyer, T. J. Kippenberg, and F. Marquardt, Rev. Mod. Phys. **86**, 1391- 1452 (2014).
- [2] N. Fiaschi, B. Hensen, A. Wallucks, R. Benevides, J. Li, T. P. Mayer Alegre & S. Gröblacher, Nat. Phot. 15, 817–821 (2021).
- [3] S. Pautrel, Z. Denis, J. Bon, A. Borne, and I. Favero, Phys. Rev. A 101, 063820 (2020).
- [4] P. Rakich and F. Marquardt, New J. Phys. 20 045005 (2018).
- [5] D. Vitali, S. Gigan, A. Ferreira, H. R. Bohm, P. Tombesi, A. Guerreiro, V. Vedral, A. Zeilinger, and M. Aspelmeyer, Phys. Rev. Lett. **98**, 030405 (2007).
- [6] Deng-Gao Lai, Jie-Qiao Liao, A. Miranowicz, and F. Nori, Phys. Rev. Lett. 129, 063602 (2022).
- [7] B.-y. Zhou, and G.-x. Li, Phys. Rev. A 94, 033809 (2016).
- [8] J. Restrepo, C. Ciuti, and I. Favero, Phys. Rev. Lett. 112, 013601 (2014).
- [9] Safavi-Naeini, A. H., T. P. Mayer Alegre, J. Chan, M. Eichenfield, M. Winger, Q. Lin, J. T. Hill, D. E. Chang, and O. Painter, Nature (London) 472, 69 (2011).
- [10] Safavi-Naeini, A. H., and O. Painter, Opt. Express 18, 14 926 (2010).
- [11] Safavi-Naeini, A. H., and O. Painter, New J. Phys. 13, 013017 (2011).
- [12] M. Schmidt, S. Kessler, V. Peano, O. Painter, and F. Marquardt, Optica 2, 635 (2015).
- [13] J. Vijayan, J. Piotrowski, C. G.-Ballesterro, K. Weber, O. Romero-Isart and L. Novotny, Nat. Phys. 20, 859–864 (2024).
- [14] M. Ludwig and F. Marquardt, Phys. Rev. Lett. 111, 073603 (2013).
- [15] G. Li, W. Nie, X. Li, and A. Chen, Phys. Rev. A 100, 063805 (2019).
- [16] B. M. Brubaker, J. M. Kindem, M. D. Urmey, S. Mittal, R. D. Delaney, P. S. Burns, M. R. Vissers, K. W. Lehnert, and C. A. Regal, Phys. Rev. X 12, 021062 (2022).

- [17] J. Piotrowski, D. Windey, J. Vijayan, C. G.-Ballesterro, A. de los Ríos Sommer, N. Meyer, R. Quidant, O. R.-Isart, R. Reimann and L. Novotny, *Nat. Phys.* 19, 1009–1013 (2023).
- [18] G. Huang, W. Deng, H. Tan1, and G. Cheng, *Phys. Rev. A* 99, 043819 (2019).
- [19] Wen-ju Gu and Gao-xiang Li, *Phys. Rev. A* 88, 013835 (2013).
- [20] S. Huang and A. Chen, *Phys. Rev. A* 103, 023501 (2021).
- [21] C. Galland, N. Sangouard, N. Piro, N. Gisin, and T. J. Kippenberg, *Phys. Rev. Lett.* 112, 143602 (2014).
- [22] N. Fiaschi, B. Hensen, A. Wallucks, R. Benevides, J. Li, T. P. Mayer Alegre and S. Gröblacher, *Nat. Photon.* 15, 817–821 (2021).
- [23] C. Zhong, Xu Han, and Liang Jiang, *Phys. Rev. Applied* 18, 054061 (2022).
- [24] C. Yang, X. Wei, J. Sheng and H. Wu, *Nat. Comm.* 11, 4656 (2020).
- [25] H. Ren, T. Shah, H. Pfeifer, C. Brendel, V. Peano, F. Marquardt and O. Painter, *Nat. Comm.* **13**, 3476 (2022).
- [26] C. Yang, X. Wei, J. Sheng, and H. Wu, *Nat. Comm.* 11, 4656 (2020).
- [27] J. del Pino, Jesse J. Slim & Ewold Verhagen, *Nat.* 606, 82-87 (2022).
- [28] H. Jing, Ş. K. Özdemir, H. Lü and F. Nori, *Sci. Rep.* 7, 3386 (2017).
- [29] P. Djorwe, Y. Pennec, and B. Djafari-Rouhani, *Phys. Rev. Applied* 12, 024002 (2019).
- [30] A. Seif, W. DeGottardi, K. Esfarjani and M. Hafezi, *Nat. Comm.* 9, 1207 (2018).
- [31] S. Raeisi, and F. Marquardt, *Phys. Rev. A* 101, 023814 (2020).
- [32] A. Mitra, *Annu. Rev. Condens. Matter Phys.* 9, 245 (2018).
- [33] H. Hu and E. Zhao, *Phys. Rev. Lett.* 124, 160402 (2020).
- [34] A. Polkovnikov, K. Sengupta, A. Silva, and M. Vengalattore, *Rev. Mod. Phys.* 83, 863 (2011).
- [35] J. Eisert, M. Friesdorf, and C. Gogolin, *Nat. Phys.* 11, 124 (2015).
- [36] T. Begzjav, J. S. Ben-Benjamin, H. Eleuch, R. Nessler, Y. Rostovtsev and G. Shchedrin, *J. Mod. Opt.* 65, 1378–1384 (2018).
- [37] Kejie Fang, Jie Luo, Anja Metelmann, Matthew H. Matheny, Florian Marquardt, Aashish A. Clerk and Oskar Painter, *Nat. Phys.* 13, 465 (2017).